Available online at www.sciencedirect.com
SCIENCE DIRECT
ELSEVIER
Colloids and Surfaces A: Physicochem. Eng. Aspects 269 (2005) 28–34
COLLOIDS AND SURFACES A
www.elsevier.com/locate/colsurfa

Ultrasonic formation of nanobubbles and their zeta-potentials in aqueous electrolyte and surfactant solutions

Sung-Ho Cho [a], Jong-Yun Kim [b], Jae-Ho Chun [a], Jong-Duk Kim [a,*]

[a] *Department of Chemical and Biomolecular Engineering, Center for Energy and Environment, Korea Advanced Institute of Science and Technology, 373-1, Guseong-dong, Yuseong-gu, Daejeon, Republic of Korea*
[b] *Nuclear Chemistry Research Division, Korea Atomic Energy Research Institute, Dukjin-dong, Yuseong-gu, Daejon 305-353, Republic of Korea*

Received 24 February 2005; received in revised form 19 June 2005; accepted 28 June 2005
Available online 16 August 2005

Abstract

The electrokinetic behaviors of nanobubbles internally generated by ultrasonication were investigated in terms of the stability of bubble, size distribution and zeta-potentials. When aqueous solutions were sonicated with a palladium electrode, stable nanobubbles having effective diameters of several hundreds nanometer were formed within a few minutes, and the sizes and size distributions remained stable for up to 1 h. The bubble sizes slightly increased when salts added and significantly reduced when surfactants added. As the chain length of alkyl group of C_nTAB increased, the size and size distribution increased with n. A micellar model was proposed to explain the formation of nanobubbles and their size reduction. Zeta-potentials of nanobubbles showed a sharp change at CMC, increasing linearly with surfactant concentrations at low concentrations and invariant at high concentrations. The surface ionization and adsorbed monolayers at a bubble surface would result in a degree of dissociation of a planar air/water interface, but the calculated degree of dissociation at the bubble surface is very low compared with that of micelles. It would be attributed to the counter ion binding at interface or curvature effect.

Keywords: Zeta-potential; Critical micelle concentration; Nanobubble; Ultrasonication; Alkyltrimethylammonium bromide

1. Introduction

Electrokinetic properties of microbubbles in aqueous solutions are of significance when equilibrium and dynamic behaviors of surface charge, lifetime and mutual interaction with other materials are evaluated. The entrapped gas bubbles in a high density liquid would emerge in many physical and chemical processes [1], while nanobubbles in liquids could deliver a microscopic level of information at liquid–gas interfaces [2]. In any cases, the adsorption of ionic substances onto an air/water interface would play a key role to enhance the efficiency of ore flotation and foam separation processes [3,4] and ultrasonic diagnosis with contrast agents [5]. Meanwhile, the image of nanobubbles was reported by a tapping mode AFM when a hydrophobic surface was immersed in water [6,7], and the time evolution of nanobubbles was by sweeping the surface of a hydrophobic glass substrate in water [8]. Nevertheless, the electrokinetic surface potentials at air/water planar interface could be hardly determined, but the zeta-potentials of bubbles dispersed in water would be directly measured. Further, relatively large and externally injected bubbles (generally greater than 1 μm) might bring about electroosmotic water transports and hydrodynamic effects and consequently make it difficult to analyze the electrophoretic mobilities [2,9–13]. However, zeta-potentials of very small bubbles, i.e., nanobubbles, internally generated with and without alkyl polyglycosides (APG) in aqueous solutions [2], were recently determined without the side effects appeared in electrophoretic measurements such as gravitational forces, convection currents, and many other non-equilibrium effects.

In this paper, we report the formation and stability of nanobubbles in aqueous solutions, which were internally generated by ultrasonication. The nucleation of a gas bubble

* Corresponding author. Tel.: +82 42 869 3921; fax: +82 42 869 3910.
E-mail address: jdkim@kaist.ac.kr (J.-D. Kim).

0927-7757/$ – see front matter © 2005 Elsevier B.V. All rights reserved.
doi:10.1016/j.colsurfa.2005.06.063

could be facilitated by the presence of dissolved gas, or of dust or ions, and surfactants would play a role in the nucleation by lowering the surface tension of aqueous solution. The dispersion stability of nanobubbles could be monitored by the bubble size, bubble density, and surface properties of bubbles. The negatively or positively charged surface depending on the pH of a solution, adsorbed ions, surfactants, and polymers, would control the stability of bubbles, the adsorption of ions, and the bubble hydrodynamics. In fact, the adsorptions, surface tensions, and zeta-potentials of nanobubble surface would be the most important factors to understand the bubble stability and dynamics.

2. Experimental

2.1. Materials

The surfactant series of alkyl trimethylammonium bromide, C_nTAB were used as purchased. C_{10}TAB (decyl trimethylammonium bromide; 98%) and C_{14}TAB (tetradecyl trimethylammonium bromide; 99%) were purchased from Fluka Co. C_{12}TAB (dodecy trimethylammonium bromide; 99%), C_{16}TAB (hexadecyl trimethylammonium bromide; 99%) were obtained from Aldrich Chemical Co. Sodium dodecyl sulfate (SDS), potassium bromide (KBr, 99%), sodium chloride (NaCl, 95%), calcium chloride ($CaCl_2$, 99%), sodium sulfate (Na_2SO_4, 99%), all of which were purchased from Aldrich. All surfactant solutions were prepared using de-ionized water (MilliQ water system, Millipore Ltd., Mississauga, Ontario). The de-ionized water had an electrical conductance of 1.5 $\mu S\,cm^{-1}$ and pH of 5.5 when it was saturated with CO_2 from air.

2.2. Preparation of nanobubble

Nanobubbles were generated by sonicating the sample solutions with a two-sided 5 mm × 10 mm palladium-coated electrode immersed. Ultrasonic energy was exerted by a Vibra-Cell sonicator (Sonic & Material Instrument) which has a frequency of 20 kHz and an output power of up to 200 W. Every aqueous sample was filtered using 0.2 μm filter (Sterile Acrodisc) for dust removal before sonication. Then, generic nanobubbles were sufficiently stable and reproducible for measurements [2].

2.3. Zeta-potential and size measurement of nanobubble

Zeta-potentials of bubbles adsorbed with surface active materials were measured by ZetaPlus (Brookhaven Instruments Co., Holtsville, New York) with Uzgiris, Brookhaven electrodes coated by palladium and He–Ne laser as a light source. Each data point for zeta-potentials was an average of 15 measurements or above at room temperature. The mobility of nanobubbles was determined from a shift in frequency of a laser Doppler spectrum. Consequently, zeta-potential (ζ) was calculated by the Smoluchowski equation:

$$\mu = \frac{\varepsilon_0 \varepsilon_w \zeta}{\eta} \quad (1)$$

where μ is the mobility ($10^{-8}\,m^2\,s^{-1}\,V^{-1}$), ε_0 is the permitivity of free space ($C^2\,J^{-1}\,m^{-1}$), ε_w is the relative permittivity of water, η is the viscosity of water ($g\,cm^{-1}\,s^{-1}$), and ζ is the zeta-potential (mV). The half width at half height of zeta-potential was less than 15 mV in all the cases.

The size of bubbles was measured by a dynamic light scattering method based on the particle size option in ZetaPlus. The scattered intensity was registered at the scattering angle of 90° and temperature of 298.15 K.

Table 1
Effective diameters of bubbles generated by sonication in pure water

Time (min)	Effective diameter (nm)
0	749
10	745
20	749
30	753
40	774
50	796

2.4. Surface tension and specific conductivity

Surface tensions were measured with a K12 tensionmeter (Krüss) equipped with a du Nouy ring. The addition of surfactants was controlled by a Metrhohm Dosimat microtitration unit system. All the experiments were repeated at least three times and an average of all the values was determined. The conductance of surfactant solutions was measured by using an Orion Model 115 conductivity meter (Orion Research Inc., MA) using a dip-type cell with cell constant 1.0 cm^{-1} and calibrated with a NaCl solution in a suitable concentration range. The measuring cell was immersed in a thermostat bath, maintaining the temperature constant within 25 ± 0.1 °C.

3. Results and discussion

3.1. Creation and stabilization of nanobubble

3.1.1. Bubble creation

Fig. 1 shows the size distribution of nano/microbubbles sonicated with a palladium electrode and Table 1 shows the effective diameters of bubbles in pure water upon storage maintaining at 750 nm without significant change of sizes within 1 h.

Table 2 shows the effective diameters of bubbles according to sonic powers and sonication time. Size of bubbles increases slightly with increasing power, from 50 to 200 W. At 70 W, bubbles significantly increase within sonication time of 6 min. Also, a tip-type sonicator efficiently generated larger bubbles than a bath-type sonicator did. It is consistent with

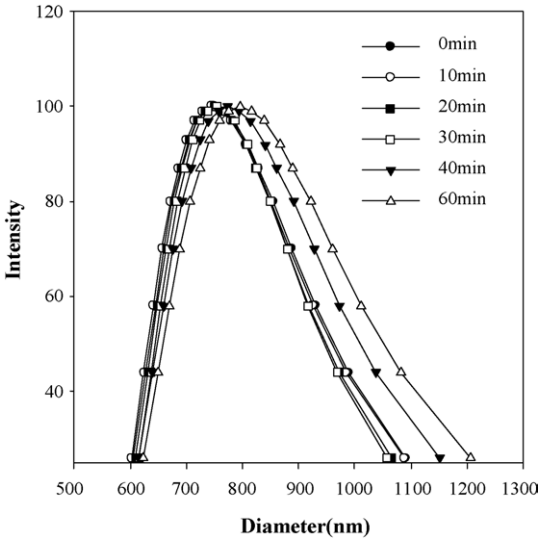

Fig. 1. Log-normal size distribution of nanobubbles prepared by sonicating the pure water with a two-sided 5 mm × 10 mm palladium-coated electrode immersed.

that a tip-type sonicator delivers a strong force required for cavitation, cleaning, explosion, and expansion. Therefore, relatively large bubbles were generated in a dip-type sonicator. The high delivery of energy into a solution would apparently enhance the formation of large cavitation in a short time and also the diffusion of volatile components into bubbles expanded the volume exponentially after an adjusting period.

Yet, the mechanism of nanobubble formation with ultrasonic energy is not clear. It is known that a high energy nucleus generated by ultrasonic energy would grow homogeneously in solution or heterogeneously on hydrophobic surfaces, followed by an equilibration between gas in bubbles and dissolved gas in water. Bubbles generated by sonic energy might oscillate with the sound frequency and survive with oscillations. At an instant during sonic compression phase, bubbles might suddenly collapse to a fraction of their maximum size. The gas inside a bubble might be thus compressed and adiabatically heated. Under certain conditions, an imploding shock wave might be driven by collapsing bubble walls, which could increase the temperature and create a rather destructive environment, and thus often used in erosion of metal surface, lithotripsy, ultrasonic cleaning, sonochemistry, and sonoluminescence. [16–21].

Table 2
Effective diameters of bubbles in pure water when sonic power and time varied

Power (for 1 min) (W)	50	100	150	200
Effective diameter (nm)	750	935	921	965
Time (70 W) (min)	0	2	4	6
Effective diameter (nm)	820	850	920	4250
Polydispersity	0.32	0.32	0.35	0.37

When bubbles are generated in a solution by ultrasonic nucleation, a microscopic void of radius, R, grows as long as the bubble pressure, P_{in}, is greater than a critical value, $P_{out} + 2\gamma/R$ calculated by the Young–Laplace equation.

$$P_{in} - P_{out} = \frac{2\gamma}{R}, \tag{2}$$

where γ is the surface tension and R is the radius. During the initial cavitation, the ultrasonic energy could be consumed to create the bubble surface and volume, $4\pi R^2\gamma + 4/\pi R^3(P_{out} - P_{in})$. After the nucleation stage, the bulk energies of bubbles would be dissipated into liquid by heat transfer through conduction and condensation and the creation of surface, and so reduced the vapor pressure P_v. If the bubble pressure would be reduced less than $P_{out} + 2\gamma/R$, the bubble would be shrunk on the assumption that no gas might be diffused or vaporized into the bubble. However, if a volatile component is diffused in the bubble, the internal pressure of bubble could be readjusted around external pressure so that the bubbles grow to rupture. The curvature effect of 750 nm bubbles at 50 W in water, $2\gamma/R$ is 3.79 atm $[2 \times 72 \times 10^{-3}\,(\mathrm{N/m})/(0.375 \times 10^{-6}\,\mathrm{m}) = 3.84 \times 10^5\,\mathrm{N/m^2} = 3.79\,\mathrm{atm}]$, while it is 2.95 atm for 200 W, where the size of bubble is 965 nm for 1 min sonication. Therefore, the total energy difference of two stable bubbles could be evaluated by $(P_{in}V + A\gamma)$;

For 750 nm bubble:

$$= (1 + 3.79) \times 1.013 \times 10^5(\mathrm{N/m^2}) \times (4\pi/3)(0.750/2 \times 10^{-6}\,\mathrm{m})^3 + 4\pi(0.750/2 \times 10^{-6}\,\mathrm{m})^2 \times 72 \times 10^{-3}(\mathrm{N/m}) = 2.34 \times 10^{-13}(\mathrm{J})$$

For 965 nm bubble:

$$= (1 + 2.95) \times 1.013 \times 10^5\,\mathrm{N/m^2} \times (4\pi/3)(0.965/2 \times 10^{-6}\,\mathrm{m})^3 + 4\pi(0.965/2 \times 10^{-6}\,\mathrm{m})^2 \times 72 \times 10^{-3}(\mathrm{N/m}) = 3.99 \times 10^{-13}(\mathrm{J}).$$

It is apparent that 965 nm bubbles require the intense energy of 1.65 times greater than that of 750 nm bubbles. Table 2 indicates that the energy conversion of sonic energy to nanobubble would not be efficient. Further, as the sonication continued, the bubble size significantly increased because of the evaporation of volatile components.

3.1.2. Growth and surface effects

The ultrasound energies would be immediately transformed into the work of cohesion by forming bubble and its surface. This process might be composed of the creation of surface, evaporation of gases to fill vacuoles, and the adsorption of impurities from bulk phase. It is extremely difficult to observe the initial creation stage and dynamics of internal pressure. Table 3 shows that the pH and ion effects on nanobubbles in solutions are relatively small. The bubble

Table 3
Effective diameter of nanobubbles in various aqueous solutions at 50 W sonication energy

pH of water	2	4	5.8	10	12
Effective diameter (nm)	749	745	749	753	774
NaCl concentration (mM)	0.001	0.01	0.1	1	10
Effective diameter (nm)	897	827	804	850	885
Na_2SO_4 concentration (mM)	0.001	0.01	0.1	1	10
Effective diameter (nm)	839	843	921	853	794
$CaCl_2$ concentration (mM)	0.001	0.01	0.1	1	10
Effective diameter (nm)	890	934	826	850	950

diameter had no dependency on pH, but it seemed that added salts increased the effective diameter 10–20% and the bubble volume 30–70%. The creation and dispersion processes of bubbles were independent of protons, nature of salts and their concentrations, but bubble sizes increased in salt solutions. Added salts reduced the solubility of volatile components like air and vapor, while slightly induced high surface tensions. Therefore, it seems that the increase of bubble sizes might be attributed to the diffusion and vaporization of volatile components.

Fig. 2 shows the effective diameters of bubbles with surfactant (SDS) concentrations at 70 W of sonication energy. Bubble sizes were reduced from 1200 to 450 nm, while the surface tension was reduced from 72 to 38 dyn/cm. The critical micelle concentration (CMC) of SDS and its surface tension were 8.2×10^{-3} M/L and 38 dyn/cm, respectively, at 25 °C [23]. The curvature effect of 450 nm bubble, $2\gamma/R$ is 3.33 atm $[2 \times 38 \times 10^{-3}(\text{N/m})/(0.45/2 \times 10^{-6}\ \text{m}) = 3.37 \times 10^5\ \text{N/m}^2 = 3.33\ \text{atm}]$, but the total energy of bubble is 4.51×10^{-14} J $[(1 + 3.33) \times 1.013 \times 10^5\ \text{N/m}^2 \times (4\pi/3)(0.45/2 \times 10^{-6}\ \text{m})^3 + 4\pi\ (0.45/2 \times 10^{-6}\ \text{m})^2 \times 38 \times 10^{-3}\ (\text{N/m}) = (2.09 + 2.42) \times 10^{-14}\ \text{J}]$. The bubble size remained invariant at three times of surfactant concentration higher than CMC. It means that three times of CMC is the proper concentration for the formation of nanobubble.

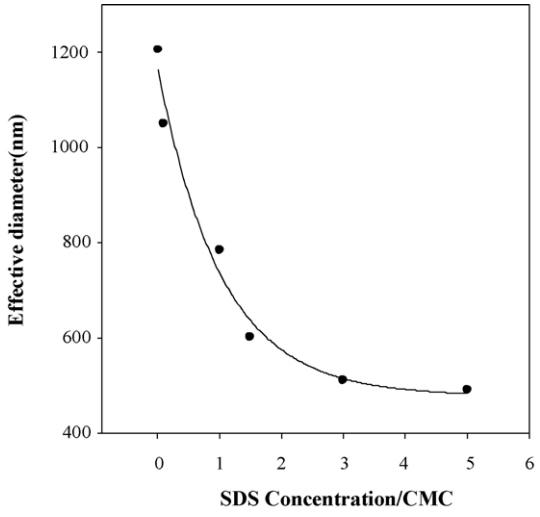

Fig. 2. Effective diameters of bubbles with SDS concentration (CMC = 8.2×10^{-3} M).

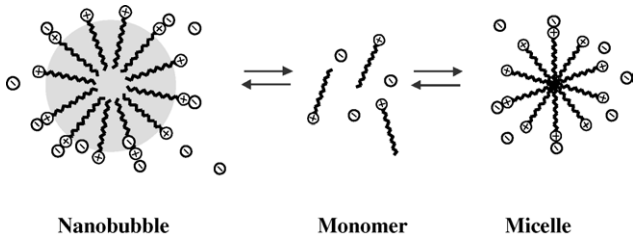

Fig. 3. Schematic representation of the stabilization of bubbles by the adsorption of surfactants and equilibrium state between fully-ionized monomers and partially-ionized micelles.

Fig. 3 shows one possible schematic diagram of an equilibrium state of surfactant monomers, micelles, and bubbles in aqueous solutions. It is postulated that bubbles could be formed by two possible pathways: cavitation in water by the intense sonic energy followed by the evaporation of water and the diffusion of surfactants, and cavitation in micelles forming air-hydrophobic interface. The former might require the high energy to create the interface, 72 dyn/cm, but surfactant molecules diffused and adsorbed at an air–water interface. Then, small bubbles would be stabilized as adsorbed surfactants. The latter might form the uniform and small bubbles at low energy sonication. The interface energy between air and hydrophobic layer is low (22.85 dyn/cm for surface tension of nonane) and the vaporization of volatile components would be limited because of surfactant layers. Then, small bubbles are stabilized from micelles. In either case, however, surfactant molecules might determine the size of nanobubble with relatively small energy.

The bubble sizes were determined at the concentration of surfactants, three times greater than CMCs. Fig. 4 shows the log-normal distribution of bubble sizes with alkyl chain length. For all cases, surface tensions were about 38–40 dyn/cm, and the size must be almost the same according to the Eq. (2). As the chain length increased, the size of nanobubbles increased such as 249 nm at $n = 10$, 231 nm

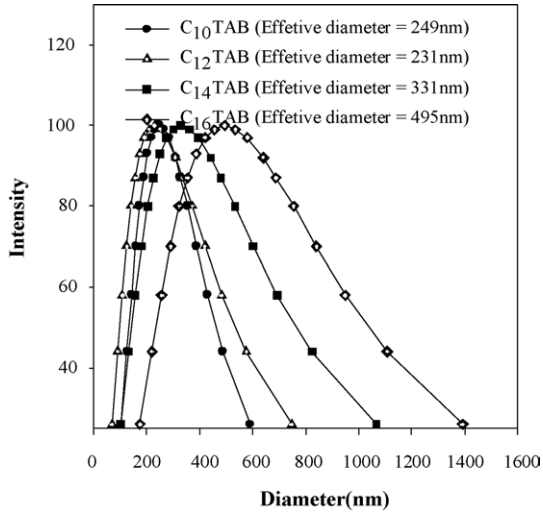

Fig. 4. Size log-normal distribution of bubbles with alkyl chain length.

at $n = 12$, 331 nm at $n = 14$, and 495 nm at $n = 16$, respectively. The thickness of their palisade layer could be estimated by $L = 0.15 + 0.1265\ n$ (n is alkyl chain length), where L is approximately the hydrophobic core length (in nm) according to the Tanford relation [23]. The thickness of nanobubbles increased with the chain length such as 1.42 nm at $n = 10$, 1.67 nm at $n = 12$, 1.92 nm at $n = 14$, and 2.17 nm at $n = 16$. The cone angles created by the chain length and hydrophilic head group would contribute to stabilize the curvature of lamellar and form bubbles.

3.2. Zeta-potentials of nanobubbles in electrolyte and surfactant solutions

Fig. 5 shows the zeta-potentials of nanobubbles in aqueous solutions of different pHs. The nanobubbles were sufficiently stable with no significant change of zeta-potentials during the measurements. The zeta-potentials of nanobubbles dispersed in a solution of 1 mM KCl were observed in a function of pH, when the size of bubbles was unchanged. At low pH, the zeta-potential was positive, but changed its sign at high pHs. The point of zero zeta-potential (isoelectric point) was located between pH 3.0 and 3.5. For pH greater than 6, zeta-potential became less than −20 mV because of the adsorption of OH^- ions. It is well recognized that the electrokinetic property of interface could be modified because of the adsorption of anions (OH^-) and the desorption of cations (H^+).

Fig. 6 shows that zeta-potentials of nanobubbles increase with salt concentrations. Since bubbles would usually bear a negative charge, an increase of NaCl solution concentration would not only cause more Na^+ ions to adsorb onto the gas–liquid interface, but also compress the electrical double layer thickness of a bubble. In the presence of bivalent Ca^{2+} ions, the zeta-potential would become less negative with $CaCl_2$ concentration than with NaCl solution. Also, it is observed that the magnitude of the bubble zeta-potential would be influenced by anion type between Cl^- and SO_4^{2-}. At dilute concentrations of bivalent anions, the zeta-potential of bubbles would be significantly negative indicating the significant selective adsorption of negative ions, but the negative mobility of each salt could be monotonically depressed with increasing concentration of each salt. Na_2SO_4 would have the more pronounced effect on the mobility than NaCl and $CaCl_2$. In low concentration, there would appear that hydration anionic energies of SO_4^{2-} were larger than that of Cl^-, but the 2:1 electrolyte was expected to produce the lower electrophoretic mobilities because of its effect on the reciprocal Debye length to that of 1:1 electrolytes at high concentration [24].

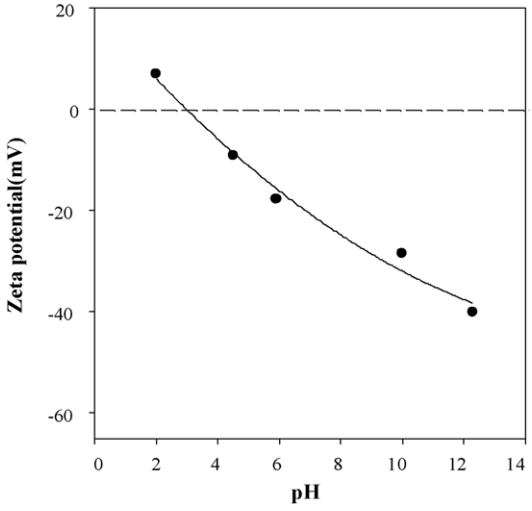

Fig. 5. The relationship between zeta-potentials of nanobubbles and pH of the water adjusted by HCl and NaOH.

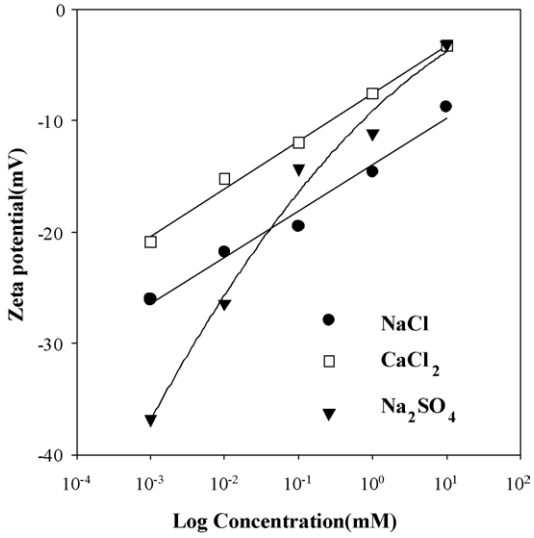

Fig. 6. Effect of electrolyte concentrations and metal ions on bubble zeta-potentials.

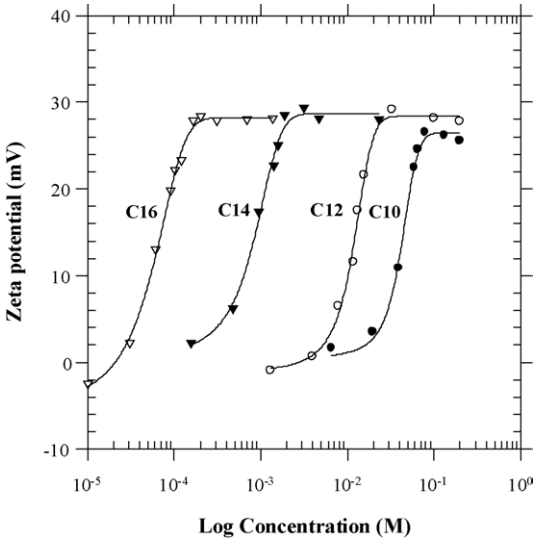

Fig. 7. Zeta-potentials of bubbles as a function of C_nTAB concentration at 0.01 M KBr solutions.

Fig. 7 shows the points of intersection of extrapolated straight line segments in a plot of the zeta-potential versus concentration, yielding apparent CMC. Zeta-potentials of C_nTAB above CMCs were in a range of 25–28 mV. Zeta-potentials of nanobubbles indicate the adsorption of surfactants, association with counter ions, and existence of free counter ions. The degree of dissociations of surfactants adsorbed on the nanobubble surface could differ from that of micelles, though there would exist dynamic equilibria among the monolayer surfactants at nanobubbles, monomeric, and micellar surfactants as shown in Fig. 3.

3.3. Adsorption and surface ionization of C_nTAB at the nanobubble surface

Fig. 7 showed zeta-potentials of nanobubbles with the concentration of ionic surfactants, C_nTAB. As its concentration increased, zeta-potentials increased linearly with log concentration, and unchanged at the concentrations greater than CMC because monolayer adsorption was completed.

In fact, nanobubbles were surrounded by an electrical double layer as ionic surfactants and electrolytes were adsorbed onto the air–water interface. The Gouy–Chapman treatment enabled the surface potential, ψ, to be related with surface charge density, σ_s of a charged surface and Debye length $1/\kappa$, and electrokinetically relevant zeta-potential ζ was often used as an approximate. Assuming that ψ is equal to ζ, the surface charge density for a 1:1 electrolyte can be calculated by the following equation [14,15]:

$$\sigma_s = \frac{2kT\varepsilon_0\varepsilon_w\kappa}{e} \sin h\left[\frac{ze\zeta}{2kT}\right] \quad (3)$$

where k is Boltzmann constant(J/K), T is absolute temperature(K), κ is the inverse of the Debye length (m^{-1}), z is the valency of ions, e is the magnitude of charge on a single electron, ε_0 is the permittivity of free space ($C^2\,J^{-1}\,m^{-1}$). ε_w is the relative permittivity of water, and ζ is the zeta-potential (V) obtained from electrophoretic mobility measurements. Alternatively, the surface number density of charged molecules can be converted to the surface charge density. The surface charge density, σ_s, at the curved air–water interface of bubbles can be expressed by the amounts of ionized surfactants [25,26]:

$$\sigma_s = e[C_nTA^+]_s \quad (4)$$

where $[C_nTA^+]_s$ is the surface concentration of dissociated surfactants. Meanwhile, the number of surfactant molecules at surface could be given as the sum of bound and unbound surfactants, designated by $[C_nTA^+]_s$ and $[C_nTABr]_s$, respectively [25,26]:

$$\Gamma = [C_nTA^+]_s + [C_nTABr]_s \quad (5)$$

Degree of surfactant dissociation at the air–water interface, α_s, can be defined by the fraction of dissociation as in the Eq. (6):

$$\alpha_s = \frac{[C_nTA^+]_s}{\Gamma} \quad (6)$$

Though C_nTAB surfactant monomers are almost ionized in a bulk solution, the ionized amounts of molecules at interface are limited as the degree of dissociation. The average number densities of molecules at interface Γ can be determined from the surface tension of air–water interface. At a dilute solution, however, ionic surfactant molecules would be completely ionized and adsorbed at interface. The adsorption of surfactants can be given by measuring the equilibrium surface tensions and from the Gibbs adsorption equation [26]:

$$\Gamma = -\frac{1}{yRT}\left(\frac{dy}{d\ \ln[C_nTAB]}\right) \quad \text{and}$$

$$y = 1 + \left(\frac{[C_nTAB]}{[C_nTAB] + [KBr]}\right) \quad (7)$$

where Γ is the surface excess of surfactant (mol/cm^2). Molecular area of surfactant at the air–water interface, A (Å), can be calculated from the Eq. (8) [26]:

$$A = \frac{10^{16}}{N\Gamma} \quad (8)$$

where N is the Avogadro number and Γ (mol/cm^2) is surface excess of surfactant. Surface excess was determined by measurements of surface tension of C_nTAB. The surface adsorption near CMC was saturated with surfactant. Table 4 shows the significant increase in maximum surface number density of C_nTAB as the chain length increased, whereas molecular area, A_{min}, were reduced from 47 to 32 Å^2, closely packed at air–water interface [27].

Degree of dissociations α_s at the bubble interface and α_s on CMC are shown in Table 5, both calculated using Eqs. (4)–(8). Shorter alkyl chains could contribute higher dissociation of molecules at the air–water interface at CMC as expected. Surfactant monomers would adsorb onto the air–water interface after binding with counter ions very strongly in a very low

Table 4
Surface excess and molecular area of C_nTAB at CMC at 0.01 M KBr

Surfactants	Γ_{max} ($\times 10^{-10}$ mol/cm^2)	A_{min} (Å^2)
C_{10}TAB	3.7	47
C_{12}TAB	4.3	39
C_{14}TAB	5.0	33
C_{16}TAB	5.2	32

Table 5
Zeta-potential, dissociation degree of air–water interface (α_s), dissociation degree of micelle (α_m) at CMC at 0.01 M KBr

Surfactants	Zeta-potential (mV)	α_s	α_m
C_{10}TAB	24.5	0.046	0.328
C_{12}TAB	26.0	0.024	0.277
C_{14}TAB	28.4	0.015	0.217
C_{16}TAB	27.9	0.013	0.176

surfactant concentration range, while surfactant monomers would reside as a fully ionized state in aqueous solutions. Counter ion dissociation of nanobubbles were compared with the degree of micellar dissociation, α_m, the ratio of the slopes above and below the CMC of C_nTAB obtained from the specific conductivity. The degree of micelle dissociation would be the fraction of surfactant molecules in micellar aggregates that do not have bound counter ions [22]. Degrees of C_nTAB micelle dissociation (α_m) in Table 5 calculated for spherical micelles were much greater than those (α_s) of adsorbed layers at the curved air–water interface. Large difference of dissociation between nanobubble and micelle might be due to the free counter ions at the diffuse double layer and curvature of the nanobubble. Conductivity is averaged over the bulk concentration of free ions and the degree of micelle dissociation (α_m) would reflect the reduction of free ions by association with micelle, while the zeta-potential would be determined by the local number density of ions near the shear plane, and the charge density of surfactants would be shielded by the free negative ions. This factor is consistent with the results of the relatively low zeta-potential, i.e., about 25 mV, while it might increase over 100 mV on silica surface at low KBr [26]. The ratio of $[Br^-]_s/[Br^-]_b$ could correspond to the Boltzmann factor, $\exp(e\zeta/kT)$, as much as 50 at 100 mV, therefore the relative concentration of free ions would be high near the interface. Another explanation would be the curvature effect of micelles. The size of nanobubbles was 330 nm for C_{14}TAB and the monolayer at the air–water interface forms packed structure. The molecular area of C_{12}TAB micelle was 118 Å^2 [28], significantly greater than the molecular area of C_{12}TAB at air–water interface, 39 Å^2 (Table 4). Therefore, the head groups of micelles exposed to the hydrophilic environment may have higher degree of dissociation.

4. Conclusions

Surfactant adsorption and ionization at the curved air–water interface was investigated in a stable nanobubbles system generated by ultrasonication with palladium electrode. Nanobubbles of 750 nm for pure water were formed with bath-type sonicator and stable for 1 h, and the sizes shifted a little with ions. As power and time of sonication increased, the size of bubble increased. Adding surfactants, the surface tension drops to 38 dyn/cm and the bubble size reduced to 450 nm. As the chain length of alkyl group of C_nTAB increased, the size increased with n. A micellar model was proposed to explain the formation of nanobubbles and size reduction. Zeta-potentials of nanobubbles showed a sharp change at CMC, increasing linearly with surfactant concentrations at low concentration and invariant at high concentration. The surface ionization and adsorbed monolayers at the bubble surface would result in a degree of dissociation of a planar air–water interface, but the calculated degree of dissociation at the bubble surface is very low compared with that of micelles. It would be attributed to the counter ion binding at interface or curvature effect.

References

[1] S.T. Lou, Z.G. Quang, Y. Zang, X.J. Li, J. Hu, M.Q. Li, F.J. Yang, Nanobubble on solid surface imaged by atomic force microscopy, J. Vac. Sci. Technolgon. B 18 (5) (2000) 2573.
[2] J.Y. Kim, M.G. Song, J.D. Kim, J. Colloid Interface Sci. 223 (2000) 285.
[3] G.H. Kelsall, S. Tang, S. Yurdakul, A.L. Smith, J. Chem. Soc., Faraday Trans. 92 (20) (1996) 3997.
[4] K. Kubota, G.J. Jameson, Jpn. J. Chem. Eng. 26 (1) (1993) 7.
[5] L. Hoff, Ultrasonics 34 (1996) 591.
[6] Phil attard, Michael P. moody, James W.G. Tyrrell, Physica A 314 (2002) 696.
[7] N. Ishda, T. Inoue, M. Miyahara, K. Higashitani, Langmuir 16 (2000) 6377.
[8] J.W.G. Tyrrell, P. Attard, Langmuir 18 (2002) 160.
[9] S. Usui, H. Sasaki, H. Matsukawa, J. Colloid Interface Sci. 81 (1978) 80.
[10] C. Li, P. Somasundaran, J. Colloid Interface Sci. 148 (1992) 587.
[11] A. Graciaa, G. Morel, P. Saulner, J. Lachaise, R.S. Schechter, J. Colloid Interface Sci. 172 (1995) 131.
[12] D. Balzer, Langmuir 9 (1993) 3375.
[13] R.H. Yoon, J.L. Yordan, J. Colloid Interface Sci. 113 (1986) 430.
[14] R.A. Horne, R.P. Young, Electrochim. Acta 17 (1972) 763.
[15] W.B. Russel, D.A. Saville, W.R. Schowalter, Colloidal Dispersions, Cambridge University Press, 1989, p. 109.
[16] C.E. Brennen, Cavitation and Bubble Dynamics, Oxford University Press, Oxford, 1995.
[17] F.R. Young, Cavitation, McGraw Hill, New York, 1989.
[18] T.G. Leighton, The Acoustic Bubble, Academic Press, London, 1994.
[19] W.T. Richards, A.L. Loomis, J. Am. chem. Soc. 49 (1927) 3086.
[20] D. Bremner, Adv. Sonochem. 1 (1990) 1.
[21] A.J. Walton, G.T. Reynolds, Adv. Phys. 33 (1984) 595.
[22] M.J. Rosen, Surfactants and Interfacial Phenomena, second ed., John Wiley & Sons, New York, 1989, p. 67.
[23] C. Tanford, The Hydrophobic Effect-Formation of Micelles and Biological Membranes, Wiley, New York, 1980.
[24] C. Yang, T. Dabros, D. Li, J. Czarnecki, J.H. Masliyah, J. Colloid Interface Sci. 243 (2001) 128.
[25] S. Nespolo, M.A. Bevan, Y.C. Chan, F. Grieser, G.W. Stevens, Langmuir 17 (2001) 7210.
[26] S.B. Johnson, C.J. Dummond, P.J. Scales, S. Nishimura, Langmuir 11 (1995) 2367.
[27] D.N. Rubingh, P.M. Holland, Cationic Surfactants; Physical Chemistry, Mercel Dekker, New York, 1990, p. 91.
[28] R. Sabate, M. Gallardo, J. Estelrich, Electrophoresis 21 (2000) 481.